Nuclear Quadrupole Resonance and the Electric Field Gradient in Metallic Indium*

R. R. HEWITT AND T. T. TAYLOR
Department of Physics, University of California, Riverside, California
(Received July 12, 1961)

The nuclear quadrupole resonance in metallic indium has been followed continuously from 4.2°K to 390.2°K and two sources of field gradient have been investigated. One of these is the usual "ionic" model involving point ions in a uniform background charge density. The contribution from this source has been calculated by a new method to seven figures at three representative a/c ratios; from these data the ionic field gradient in indium at any submelting temperature can be inferred.

Since the ionic contribution accounts for only about 20% of the observed field gradient, a second source has been considered. This source is an undulatory component of charge density having the periodicity of the lattice. It is found that a modest amount of this undulatory component does produce sufficient field gradient to explain the observations.

I. INTRODUCTION

THE investigation of the interaction of the nuclear electric quadrupole with the local electric field gradient (EFG) in metals was initiated[1] with the hope of obtaining, ultimately, more detailed information about the structure of metals in general and about the spatial distribution of the conduction electrons in particular.

Indium has a relatively simple body-centered tetragonal structure which departs sufficiently from cubic symmetry to produce a substantial EFG. It was chosen for this study in the hope that the sources of this EFG could be easily identified with (1) the ionic array and (2) the continuous charge density corresponding to the distribution of conduction electrons. The spectrum of the nuclear quadrupole resonance (NQR) in indium has been observed independently by two groups.[2,3] This paper is a more detailed account of the work reported in reference 2 and is an extension of that work especially in regard to the calculation of the EFG.

Any study of the quadrupolar interaction begins with the expression of the potential energy of orientation of an electric quadrupole characterized by its tensor components Q^{ij} in a field derived from the potential $V(x^i)$. Thus,

$$E=\tfrac{1}{2}(\partial^2 V/\partial x^i \partial x^j)Q^{ij}. \tag{1.1}$$

Since the same constant can be subtracted from each of the diagonal elements of the field gradient matrix without changing the relative orientational energy, it is usual in (1.1) to work with a traceless matrix corresponding to only the Laplacian portion of the potential. If the quadrupole in question is an atomic nucleus with intrinsic spin I, its orientation is known only in terms of its nuclear angular momentum state and (1.1) must be transformed[4] into a Hamiltonian composed of angular momentum operators. If, as in the present case, the EFG is axially symmetric with respect to the x^3 or z axis, the energy levels associated with this Hamiltonian can be expressed explicitly[5] in terms of I and its projection M:

$$E_M=\frac{|e^2qQ|}{4I(2I-1)}[3M^2-I(I+1)], \tag{1.2}$$

where Q is the conventional designation for the nuclear quadrupole moment, and eq is the second z derivative of the Laplacian portion of the potential at the site of the nucleus. Transitions between adjacent M levels as given by (1.2) account for the observed NQR spectrum in this case of axial symmetry.

It is essential to distinguish between the EFG at the site of the nucleus, that is eq, and the EFG in which the entire ion to which this nucleus belongs, is situated. The latter EFG, here designated eq_0, is produced by all charge not associated with the ion and can be calculated provided that the location of all such charge is known. Thus an hypothesis concerning the total crystal charge distribution can be tested with regard to its ability to generate a reasonable value of eq_0. The relationship between eq and eq_0 is a numerical one given by the Sternheimer antishielding factor[6]:

$$eq=(1-\gamma_\infty)eq_0. \tag{1.3}$$

A recent calculation[7] of $(1-\gamma_\infty)$ for the indium +++ ion yields a value of 16.33. This value is used in all calculations here.

Equation (1.3) assumes that the distortion of an ion core by the action of other charge takes place primarily as a result of the Laplacian component of the field generated by such charge. In other words, the distor-

* Work supported in part by the National Science Foundation.
[1] W. D. Knight, R. R. Hewitt, and M. Pomerantz, Phys. Rev. **104**, 271 (1956).
[2] R. R. Hewitt and W. D. Knight, Phys. Rev. Letters **3**, 18 (1959).
[3] W. W. Simmons and C. P. Slichter, Phys. Rev. **121**, 1580 (1961).
[4] M. H. Cohen and F. Reif, in *Solid-State Physics*, edited by F. Seitz and D. Turnbull (Academic Press, Inc. New York, 1957), Vol. 5, pp. 329–332.
[5] T. P. Das and E. L. Hahn, in *Solid-State Physics*, edited by F. Seitz and D. Turnbull (Academic Press, Inc., New York, 1958), Suppl. 1, p. 5.
[6] T. P. Das and R. Bersohn, Phys. Rev. **102**, 733 (1956).
[7] G. Burns and E. G. Wikner, Phys. Rev. **121**, 155 (1961).

tion takes place *as if* all other charge were totally external to the ion, even though the actual situation is known to be otherwise. The potential of a charge distribution which actually penetrates the ion core can be written in an expansion with surface harmonic angular dependence and complicated radial dependence as in Eq. (A19) of Appendix A. The radial dependence associated with a given surface harmonic of order l, however, begins with the power r^l and includes only higher powers. It follows that, within the framework of a particular surface harmonic, the Laplacian term is the most important. This remark argues in favor of the stated assumption. It is of course possible that the ionic distortion produced by the $r^2P_0(\cos\theta)$ term, for instance, will affect the amount of distortion produced by the $r^2P_2(\cos\theta)$ term. The present belief of the authors is that such cross-coupled effects between different surface harmonic species are relatively small and that therefore (1.1) can, at least tentatively, be used.

The present report includes a description of the experimental methods and results, the calculation of eq_0 and eq, a comparison of the temperature dependence of the experimentally determined eq and the calculated values, and finally a discussion of the several areas of uncertainty which remain and of the research efforts which are intended to help resolve them.

II. EXPERIMENTAL METHOD

The NQR measurements were made with a variable frequency marginal oscillator similar to the Pound-Knight[8] oscillator. The resonance was modulated with an on-off magnetic square wave of about a 100-oe amplitude. The modulated signal was detected with a narrow-band, phase-sensitive detector and displayed on a recording potentiometer. In some measurements at 4.2°K and below, frequency modulation with a variable capacity silicon diode in the tank circuit was used instead of the field modulation.

Frequency measurements in the case of the field modulation were made by beating a BC 221 frequency meter against the sweeping frequency of the marginal oscillator. In the case of frequency modulation, a Hewlett-Packard model 524C electronic counter was used with a sufficient gating time to provide the desired accuracy. All frequency markers were made with a precision of ±100 cps. The frequency meters were calibrated against a cesium atomic clock.

The samples were metal powders mixed with an equal volume of quartz powder. A 20-g sample of 325 mesh indium powder was used for the 77°K to room temperature measurements and below 77°K a sample of 2-μ diameter spheres was used. These spheres were produced by melting and sonorating an indium ingot in a decane solution; this metal powder was mixed with the quartz powder and then evaporated to dryness. The initial sample contained about 2 g of metal, but a second sample of about 10 g of metal was used for the temperature range of 4.2° to 77°K. The size and uniformity of the particle sizes was monitored with an oil immersion microscope. All of the indium used had a reported purity of 99.999% and was purchased from the Indium Corporation of America.

The sample was located in a double Pyrex Dewar, and the temperature was varied by allowing the helium in the inner Dewar to evaporate to the liquid nitrogen temperature of the outer Dewar. The rate of temperature change was about 4 K° per hour and allowed resonance measurements at about every 1 K°. In the range of 77° to 55°K, a number of measurements were made by pumping on nitrogen placed in the inner Dewar. A similar method of varying the temperature in the range 78°K to room temperature was used in allowing the liquid nitrogen to evaporate and making measurements as the sample warmed to room temperature. In all cases a thermocouple was immersed in the powdered sample, and temperatures were recorded at about two minute intervals to the nearest 0.1°K, allowing a continuous temperature monitor while the resonance was being recorded. The thermocouple used below 77°K was made of AgAu-AuCo alloys and had been carefully calibrated against a copper-constantan thermocouple. A copper-constantan thermocouple was used above 77°K. The temperature measurements at room temperature and below fit smoothly to the precision of measurement, about ±2 kc/sec, and in overlapping regions the different sets of measurements were in excellent agreement, the points being within the scatter of ±2 kc/sec.

For room temperatures and above a 9-g sample of 325 mesh indium powder in mineral oil was used. The heating was provided by a bifilar heater wire wound about the rf shield can and again the temperature was monitored by a copper-constantan thermocouple imbedded in the sample. Due to the poorer signal to noise ratio at these higher temperatures, the uncertainty of measurement of the central frequency was increased to ±5 kc/sec.

III. RESONANCE FREQUENCIES AND LINE WIDTHS

From the energy level arrangement of Eq. (1.2), it is seen that the resonant frequency for the transition in which the magnitude of the projection quantum number increases by one to a final value $|M_f|$, is given by:

$$\nu=\frac{|e^2qQ|}{4I(2I-1)h}3(2|M_f|-1). \tag{2.1}$$

The two isotopes In^{113} and In^{115}, with natural abundances of 4.16% and 95.84% respectively, each have a nuclear spin of 9/2 giving rise to four resonance lines whose central frequencies are in the ratio of 1:2:3:4. The nuclear quadrupole moments of In^{113} and In^{115} have been measured by atomic beam techniques[9] as

[8] R. V. Pound and W. D. Knight, Rev. Sci. Instr. **21**, 219 (1950).

[9] H. Taub and P. Kusch, Phys. Rev. **75**, 1481 (1949).

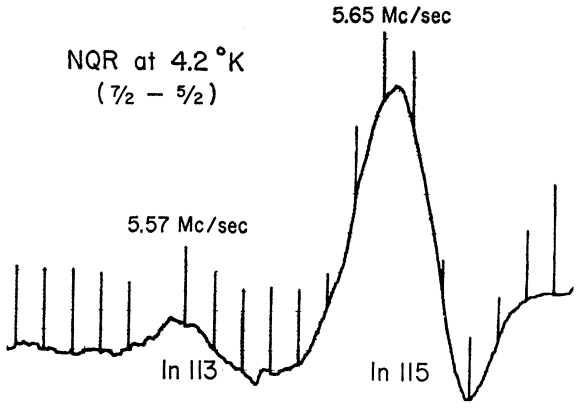

FIG. 1. Recorder trace of the $(5/2 \rightarrow 7/2)$ transition resonance of In^{113} and In^{115} at 4.2°K.

1.144 and 1.161×10^{-24} cm^2 respectively and these two sets of four resonances from the two isotopes should be in the ratio of 1.144 to 1.161. Figure 1 is a photograph of the recorder trace of the $(5/2 \rightarrow 7/2)$ transition, this resonance is of the two gram sample of 2 micron spheres at 4.2°K. The two isotopes are easily discerned here.

The central frequencies of the four resonances of the most abundant isotope at 4.2°K are shown in Table I. The ratio of the resonances are shown to demonstrate the accuracy of the measurement; these ratios should be 1:2:3:4. The half intensity line widths are also shown in Table I. It should be pointed out in Fig. 1 that there is a marked asymmetry in the line shape. This asymmetry is more pronounced in the $(7/2 \rightarrow 9/2)$ resonance, less pronounced in the $(3/2 \rightarrow 5/2)$ resonance and not detectable in the $(1/2 \rightarrow 3/2)$ resonance. This asymmetry is not believed to be due to strains since it has been observed in several samples and has this same character. Phase shifts associated with skin-depth problems are also ruled out since the particles are only 2 microns in diameter. Paramagnetic impurities would broaden the resonance in a Gaussian manner and would not be expected to provide any asymmetry. The increasing asymmetry with increasing $|M_f|$ values implies that the asymmetry is dependent on the orientation in the crystal. The asymmetry is not a property of the modulation since it has been observed both by magnetic field modulation and frequency modulation. The asymmetrical character of the resonance line disappears at about the Debye temperature (109°K). $|e^2qQ/h|$ from the 4.2°K data shown in Table I and from equation (2.1) is 45.24 ± 0.01 Mc/sec where the ± 0.01 Mc/sec is obtained from the scatter in these four measurements.

The resonance of highest intensity, the $(5/2 \rightarrow 7/2)$ resonance was chosen to trace the temperature dependence of this interaction. These measurements of the frequency of the $(5/2 \rightarrow 7/2)$ transition as a function of temperature and the proportional quadrupole coupling $|e^2qQ/h|$ are plotted in Fig. 2. Several values of $|eq|$ obtained from these measurements are tabulated in Table III in the next section for comparison with the calculated EFG. Except for the disappearance of the resonance asymmetry, no change in line widths was observed throughout this temperature range.

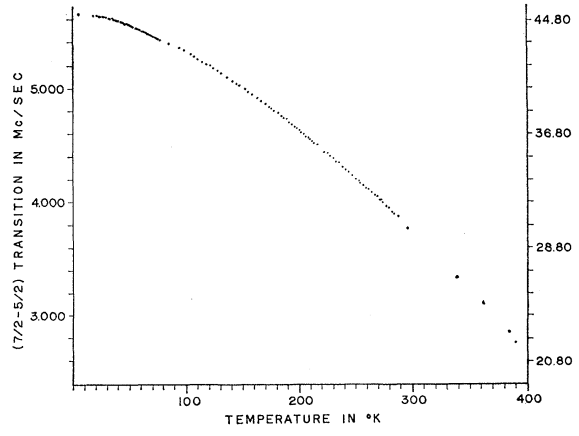

FIG. 2. Central frequency of the $(5/2 \rightarrow 7/2)$ transition of In^{115} as a function of temperature; the proportional quadrupole coupling $|e^2qQ/h|$ is plotted as the alternate ordinate.

TABLE I. Indium NQR transitions, multiples, and line widths at 4.2°K.

Transition	Frequency (Mc/sec)	Multiple	Half-intensity linewidth (kc/sec)
$(1/2 \rightarrow 3/2)$	1.886 ± 0.002	1.0000	33.5 ± 3.0
$(3/2 \rightarrow 5/2)$	3.770 ± 0.005	1.9984	22.0 ± 3.0
$(5/2 \rightarrow 7/2)$	5.655 ± 0.002	2.9984	27.9 ± 3.0
$(7/2 \rightarrow 9/2)$	7.533 ± 0.005	3.9942	24.1 ± 3.0

IV. EFG CALCULATED FROM THE IONIC MODEL

The ionic model is a term applied to an extremely simplified model for the charge distribution associated with the indium crystal structure. This model comprises a body-centered tetragonal lattice (with lattice parameters a, a, c) of monopolar positive ions each having charge $N_v e$, where N_v is the number of valence electrons per ion, plus a uniform compensating background density ρ_0 equal to $-2N_v e/a^2 c$. The ion cores are the smallest details of the charge density recognized in the construction of this model and are regarded as points in the calculation of the EFG. It follows that the EFG so determined is that in which the ion core as a whole is situated. Since this EFG is derived from the ionic model, it will be denoted eq_{0i} and the corresponding quantity at the nuclear site will be denoted eq_i.

The calculation method used here requires that the charge density be expressed as a Fourier series. If the general reciprocal lattice vector is expressed in terms

of three integral indices p_j,

$$\mathbf{h}=(p_1/a,p_2/a,p_3/c), \tag{4.1}$$

the desired series becomes

$$\rho=\text{ions}+\rho_0$$
$$=\frac{N_v e}{a^2 c}\sum_{\mathbf{h}}{}'\,[1+(-1)^{p_1+p_2+p_3}]\exp(2\pi i\mathbf{h}\cdot\mathbf{r}). \tag{4.2}$$

Here the sum is taken over all $\mathbf{h}$ vectors with the exception of $\mathbf{h}=0$. The value of eq_{0i} is twice the spherical harmonic coefficient C_2^0 given by Eq. (A16) in Appendix A. Therefore:

$$eq_{0i}=2C_2^0=(N_v e/a^2 c)(-8\pi/3)$$
$$\times\sum_{\mathbf{h}}{}'\,[1+(-1)^{p_1+p_2+p_3}]$$
$$\times\Lambda_{n+\frac{1}{2}}(2\pi h r_1)P_2(\cos\theta_{\mathbf{h}}). \tag{4.3}$$

The function $\Lambda_\nu(z)$ is defined in (A14). The sum in (4.3) has the unusual property of being independent of the

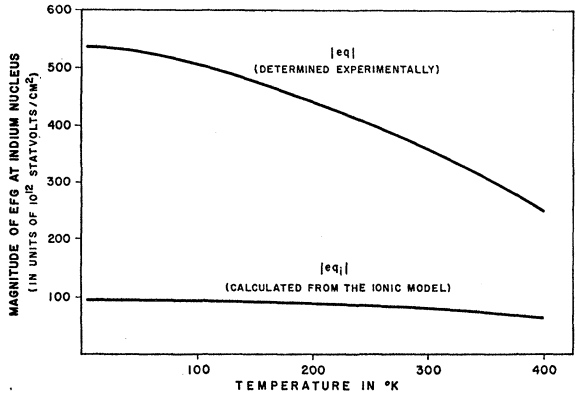

FIG. 3. Magnitude of the EFG at the indium nucleus (1) as determined experimentally and (2) as calculated from the ionic model.

values of n or of r_1, so long as r_1 is less than the nearest neighbor distance, and it correctly represents eq_{0i} provided that this condition is fulfilled. The respective values of 20 and $a(30)^{\frac{1}{2}}/2\pi$ chosen for these parameters were therefore selected for reasons of computational convenience. The results of the calculations are given in terms of dimensionless ratios in Table II.

It is possible to obtain interpolated results with nearly five-figure accuracy at any a/c ratio which falls within the range of Table II. In this way, the tabulated results have been compared with the independent calculations of deWette[10] and agreement to this order of accuracy was found to exist.

Using $N_v=3$ and available data on the temperature dependence of a and c in the range 100° to 400°K,[11] and also at 4.2°K,[12] together with the interpolation

[10] F. W. deWette, Phys. Rev. **123**, 103 (1961).
[11] J. Graham, A. Moore, and G. V. Raynor, J. Inst. Metals **84**, 86 (1955).
[12] C. S. Barrett (private communication).

TABLE II. Calculated values of the EFG in a body-centered tetragonal lattice based upon the ionic model. Lattice parameters are a, a, c; N_v is the number of valence electrons per ion and eq_{0i} is the EFG in which the ion as a whole is situated.

$(a/c)^2$	a^2ceq_{0i}/N_ve
0.42	−0.2328772
0.43	−0.1894397
0.44	−0.1508423

technique mentioned above, it was possible to arrive at the data given in Table III. Note that this table also contains the magnitude of eq as determined from the experimental data. When both $|eq_i|$ and $|eq|$ are plotted with respect to temperature as in Fig. 3, it is seen that the EFG calculated from the ionic model fails to account for the observed EFG by nearly an order of magnitude. The authors were led, therefore, to consider modifying this model by superposing an undulatory component upon the uniform charge density background ρ_0. The modification is discussed in the next section.

V. EFFECT OF AN UNDULATORY BACKGROUND COMPONENT

The modified charge density discussed in this section is not intended as a permanent substitute for a well-founded quantum mechanical model of the conduction electrons. Its introduction is merely an exploratory gesture to determine if a modest departure from uniformity in the background density of the ionic model can produce an appreciable change in the calculated EFG. The results show that a relatively small change in this background does indeed produce a large change in the EFG.

The background component ρ' selected for addition to the ionic model is defined to be proportional to the sum of the twelve lowest ordered Fourier terms in Eq. (4.2). This sum is a function with a definite, smoothly undulating, form which reflects the periodicity of the lattice and which reaches a maximum at each ion site.

TABLE III. Lattice parameters[a] and EFG in indium as functions of temperature. The quantity eq_{0i} is interpolated from Table II; eq_i is obtained from the latter by using $(1-\gamma_\infty)=16.33$.[b] Magnitude of eq as determined experimentally is also tabulated.

T (°K)	a (A)	c (A)	eq_{0i} (cgs esu)	eq_i (cgs esu)	$\lvert eq_{\text{expt}}\rvert$ (cgs esu)
4.2	3.221	4.933	-5.766×10^{12}	-94.15×10^{12}	537.5×10^{12}
100.0	3.227	4.936	-5.616×10^{12}	-91.70×10^{12}	505.4×10^{12}
150.0	3.232	4.941	-5.538×10^{12}	-90.43×10^{12}	475.3×10^{12}
200.0	3.238	4.945	-5.408×10^{12}	-88.31×10^{12}	440.5×10^{12}
250.0	3.245	4.947	-5.212×10^{12}	-85.11×10^{12}	399.8×10^{12}
300.0	3.253	4.947	-4.937×10^{12}	-80.62×10^{12}	356.2×10^{12}
350.0	3.263	4.944	-4.574×10^{12}	-74.70×10^{12}	306.9×10^{12}
400.0	3.275	4.939	-4.120×10^{12}	-67.29×10^{12}	254×10^{12} [c]

[a] Parameters at 4.2°K by C. S. Barrett (reference 12); at 100° to 400°K by Graham, Moore, and Raynor (reference 11).
[b] By Burns and Wikner (reference 7).
[c] Extrapolated from measurements ending at 390.2°K.

TABLE IV. Values of the p_j indices describing the twelve reciprocal lattice points associated with the undulatory background component ρ'.

p_1	p_2	p_3
1	0	1
0	1	1
−1	0	1
0	−1	1
1	1	0
1	−1	0
−1	1	0
−1	−1	0
1	0	−1
0	1	−1
−1	0	−1
0	−1	−1

Like the lattice itself, these maxima are somewhat asymmetrical; they will have a more gentle curvature in the z direction than in the x or y directions for cases in which c/a is greater than unity. It is precisely this feature of the undulation which makes it possible for ρ' to generate an EFG. A multiplicative parameter ζ is incorporated in the definition of ρ' in order to specify the amplitude of undulation. Thus:

$$\rho'=\zeta\frac{N_v e}{a^2c}\frac{1}{12}\sum_{12\text{ points}}\exp(2\pi i\mathbf{h}\cdot\mathbf{r}). \tag{5.1}$$

Note that ρ' attains the value $\zeta N_v e/a^2c$ at each ion site. The actual values of the p_j indices for the twelve points are given in Table IV and ρ' itself can be written in terms of real functions as follows:

$$\rho'=\zeta(N_v e/a^2c)\times\tfrac{1}{3}[\cos(2\pi x/a)\cos(2\pi y/a)+\cos(2\pi y/a)\cos(2\pi z/c)+\cos(2\pi z/c)\cos(2\pi x/a)]. \tag{5.2}$$

Although ρ' has zero average value, its maximum and minimum values are, paradoxically, not equal in magnitude. A detailed inspection shows that the quantity in square brackets above attains a maximum value of $+3$ at the ion sites and a minimum value of -1 upon a set of straight lines parallel to the unit cell edges and located midway between the ion sites. For brevity, this system of lines will be denoted by the symbol σ.

When the undulatory background component is added to the ionic model, the total background becomes $\rho'-2N_v e/a^2c$. Since this density represents electrons, it must not become positive anywhere in the unit cell; the amplitude of undulation is therefore clearly limited. Quantitatively, this means that the coefficient ζ must lie in the interval:

$$-6\leq\zeta\leq+2. \tag{5.3}$$

Negative values of ζ correspond to cases in which the electron density is relatively enhanced at the ion sites; positive values, to cases in which the electron density is relatively depleted at the ion sites and enhanced upon σ.

The EFG generated by the undulatory component ρ' just outside an ion site will be called eq_{0u} and that at a nuclear site, eq_u. This time, eq_{0u} is twice the $C'_{20}{}^0$ coefficient given by equation (A22) is Appendix A. Thus

$$eq_{0u}=2C'_{20}{}^0=\frac{\zeta}{12}\frac{N_v e}{a^2c}\left(\frac{-8\pi}{3}\right)\sum_{12\text{ points}}P_2(\cos\theta_{\mathbf{h}}). \tag{5.4}$$

The sum is an algebraic function of a/c and eq_{0u} becomes:

$$eq_{0u}=\zeta\frac{N_v e}{a^2c}\frac{4\pi}{3}\frac{1-(a/c)^2}{1+(a/c)^2}. \tag{5.5}$$

It was decided that a calculation should be made at the 4.2°K point to determine what value of ζ would yield a total nuclear EFG equal in magnitude to that observed experimentally. At this temperature, $(a/c)^2=0.4263$ and

$$eq_u=\zeta(774.5\times10^{12}\text{ statvolts/cm}^2). \tag{5.6}$$

Using data from Table III, the following equation is obtained:

$$-94.15+774.5\zeta=\pm537.5. \tag{5.7}$$

If eq is assumed to be positive, the value of ζ required is 0.816. On the other hand, if eq is assumed to be negative, the ζ value needed is only -0.572. In either event, ζ is well within the limits of -6 and $+2$ established earlier, which means that, especially in the case of the -0.572 value, the required undulation is small in comparison with the maximum possible undulation. In the first case, in which $\zeta=0.816$, the conduction electron density is minimum at the ion sites with a value equal to 0.59 times the average background density; it is maximum on σ with a value equal to 1.14 times the average. In In the second case, in which $\zeta=-0.572$, the conduction electron density is maximum at the ion sites with a value equal to 1.29 times the average value; it is minimum on σ with a value of 0.90 times average.

VI. DISCUSSION

This article shows that the theoretical explanation of the observed EFG at the indium nucleus is still in an imperfectly developed state; directions in which future progress may be expected will now be discussed.

Within the frame work of the ionic model itself, certain avenues for improved understanding remain open. It is felt, for instance, that the weak temperature dependence of $|eq_i|$ as illustrated in Table III and in Fig. 3, is not realistic and that a faster decay of this quantity with increasing temperature would appear if the thermal motions of the ions were taken into account. The average effects of these motions could be calculated using the Debye approximation in the summation of lattice modes with the aid of the elastic constants that have been measured from 1.4° to 300°K

by the ultrasonic pulse technique.[13] Another defect in the ionic model is the assumption that each ion is, in its external effects, a monopole. Actually, each ion possesses an induced quadrupole moment as a result of the EFG in which it is situated, and these induced moments will, in turn, have an effect upon the EFG in a manner analogous to the action of an ordinary polarized dielectric. The extent of this effect is being investigated.

Although the ionic contribution is by no means negligible, it is believed that the predominant source of the EFG is to be found in the non-uniform charge density associated with the extra-ionic or conduction electrons. Strong evidence for this point of view has been presented in Section V. It is hoped that the plausible but somewhat arbitrary undulatory background component presented there can be replaced by a better model, and an attack upon this problem using a method which has been applied to the conduction electron distribution problem in beryllium[14] is planned for the near future. Further evidence of the importance of the conduction electron contribution to the EFG is provided by the 10 kc/sec frequency shift observed in the indium NQR at the onset of superconductivity.[15]

Any successful conduction electron model must vary considerably with respect to temperature in order to explain the strong temperature dependence of the indium NQR which is actually observed. The electron density may vary in response to changes in the lattice parameters, and it may vary as a result of electron-phonon interactions. These two effects should be separable by pressure dependence measurements provided that the lattice parameters are known as functions of pressure. Measurements of this nature are now in progress and will be reported at a later date. The long mean free path of conduction electrons at low temperatures suggests that the effects of impurities on the NQR and the temperature dependence of these effects should provide information relevant to the conduction electron model. Experiments to determine the effects of alloying indium with dilute concentrations of other metals are being initiated.

ACKNOWLEDGMENTS

The authors are happy to acknowledge the efforts of Glenn A. Scharp of the U. S. Naval Ordnance Laboratory of Corona, California, in constructing the fine-grained table of $\Lambda_{45/2}(\sqrt{u})$ mentioned in Appendix A. This table has been an extremely valuable tool in all calculations based upon the ionic model such as, for instance, those reported with seven figure accuracy in Table II. In the construction of the Λ table, Mr. Scharp was assisted by Mayor Levine and Cliff Qualls, also of the Naval Ordnance Laboratory, and by Leo Padlog of International Business Machines. The authors also acknowledge the work of Miss Diane M. Tait in checking the results given in Table II.

The lattice parameters for indium at 4.2°K, used in Table III, were furnished prior to publication by Dr. C. S. Barrett of the University of Chicago. The private communications containing these and other data resulting from Dr. Barrett's work on the indium lattice parameters are greatly appreciated.

APPENDIX A: EXPANSION OF THE ELECTROSTATIC POTENTIAL IN A CRYSTAL

This appendix contains a derivation of the mathematical methods used in calculating the electric field gradients discussed earlier in this article. These methods are suited to a variety of crystal potential problems and are developed with wide applicability in mind. Cgs electrostatic units are employed throughout.

Any model for the charge density distribution within a crystal will, in general, include a lattice of singularities immersed in a continuous background, the whole having vanishing average value within a unit cell. The singularities may be monopoles, dipoles, multipole charge aggregations of higher order, or combinations of these. The continuous background may be absent altogether; it may be uniform; or it may be a complicated function depending upon the sophistication of the model.

At the beginning it is convenient to separate the total charge distribution into two distinct partial distributions, each of which has vanishing average value within a unit cell and each of which is assumed to be known in the form of a Fourier series. The first such partial distribution, denoted by ρ, consists of the singularities and the *uniform* component of the background. This uniform component, ρ_0 is simply the negative of the total monopole content of a unit cell divided by the volume of that cell. In terms of its Fourier series, ρ can be written

$$\rho = \text{singularities} + \rho_0 = \sum_{\mathbf{h}} A(\mathbf{h}) \exp(2\pi i \mathbf{h}\cdot\mathbf{r}). \quad \text{(A1)}$$

Here the symbol $\mathbf{h}$ represents a vector in reciprocal space and $A(\mathbf{h})$ is the Fourier coefficient. It may be remarked that the finding of $A(\mathbf{h})$ is practically a routine matter once the positions and multipolar compositions of the singularities have been specified. The second partial distribution, denoted by ρ', includes all of the charge not represented by (1), namely the *nonuniform* component of the background. In Fourier series representation, ρ' becomes:

$$\rho' = \sum_{\mathbf{h}} A'(\mathbf{h}) \exp(2\pi i \mathbf{h}\cdot\mathbf{r}). \quad \text{(A2)}$$

Since both ρ and ρ' have vanishing average value, both $A(0)$ and $A'(0)$ are equal to zero.

It is important to realize that series (A1), which represents singularities, has a very slow rate of convergence; that is, relatively many terms are needed to give a

[13] B. S. Chandrasekhar and J. A. Rayne, Scientific Paper 025-6000-P5, Westinghouse Research Laboratories, 1961 (unpublished).
[14] M. Pomerantz and T. P. Das, Phys. Rev. **119**, 70 (1960).
[15] R. H. Hammond and W. D. Knight, Phys. Rev. **120**, 762 (1960).

satisfactory approximation to the charge density ρ. On the other hand, series (A2), which represents a comparatively smooth function, has a much more rapid rate of convergence. This difference in convergence properties, plus the necessity of deleting the effect of the singularity at the origin in (A1), requires the use of entirely different methods for the calculation of the potentials generated by the respective partial charge distributions.

Attention is now directed to the potential V generated by the partial distribution ρ. For convenience, the origin of coordinates is chosen to coincide with the point at which the expansion of this potential is to be developed. It will be assumed, for generality, that this expansion point coincides with one of the singularities of (A1); the results can be specialized easily to the case in which this is not true, however. Evidently, V is representable by a series of the form

$$V=\frac{-2\pi}{3}\rho_0 r^2+\sum_{l=0}^{\infty}\sum_{m=-l}^{l}[B_l{}^m r^{-(l+1)}+C_l{}^m r^l]\times P_l{}^{|m|}(\cos\theta)e^{im\phi}, \quad \text{(A3)}$$

in the open interval $0<r<r_0$, where r_0 is the distance from the origin to the nearest neighboring singularity. The term containing $\rho_0 r^2$ is the result of an integration of Poisson's equation from the origin outward and is the only non-Laplacian term in (A3). The terms containing the $B_l{}^m$ coefficients constitute the self-potential generated by the singularity at the origin and the coefficients themselves are related to the known multipolar composition of this singularity. Thus $B_0{}^0$ is the monopole moment or net charge; $B_1{}^{-1}$, $B_1{}^0$, and $B_1{}^1$ characterize the dipole moment, etc. The terms containing the $C_l{}^m$ coefficients constitute the Laplacian component of the potential generated by all of ρ which is not associated with the singularity at the origin. This is the part of V which is of greatest interest, and one of the present objectives, therefore, is to develop a method for finding the $C_l{}^m$ coefficients. Note that the fact that V is real implies that $B_l{}^{-m}=B_l{}^{m*}$ and $C_l{}^{-m}=C_l{}^{m*}$ and conversely.

In view of the fact that V and ρ are connected by Poisson's equation, the Fourier series for the former must be

$$V=4\pi\sum_{\mathbf{h}}\frac{A(\mathbf{h})}{(2\pi h)^2}\exp(2\pi i\mathbf{h}\cdot\mathbf{r}). \quad \text{(A4)}$$

Now let the spherical polar coordinates h, $\theta_{\mathbf{h}}$, and $\phi_{\mathbf{h}}$ be associated with the reciprocal lattice vector $\mathbf{h}$. By a well-known expansion,

$$\exp(2\pi i\mathbf{h}\cdot\mathbf{r})=\sum_{l=0}^{\infty}\sum_{m=-l}^{l} i^l(2l+1)j_l(2\pi hr)\times\frac{(l-|m|)!}{(l+|m|)!}P_l{}^{|m|}(\cos\theta)P_l{}^{|m|}(\cos\theta_{\mathbf{h}})\times\exp[im(\phi-\phi_{\mathbf{h}})]. \quad \text{(A5)}$$

In this expansion, $j_l(2\pi hr)$ is a spherical Bessel function of the first kind and order l. Combining (A3), (A4), and (A5), and equating coefficients for the surface harmonic of order l and m, one obtains

$$(-2\pi/3)\rho_0 r^2\delta_{0l}+B_l{}^m r^{-(l+1)}+C_l{}^m r^l=4\pi i^l(2l+1)\times\frac{(l-|m|)!}{(l+|m|)!}\sum_{\mathbf{h}}\frac{A(h)}{(2\pi h)^2}j_l(2\pi hr)P_l{}^{|m|}(\cos\theta_{\mathbf{h}})\times\exp(-im\phi_{\mathbf{h}}). \quad \text{(A6)}$$

Here δ_{0l} is equal to unity if $l=0$ and to zero otherwise. In principle, the unknown coefficient $C_l{}^m$ can be found by inserting any fixed value of r, say r_1, $0<r_1<r_0$, into both sides of (A6) and summing over $\mathbf{h}$, that is, by performing a summation entirely in reciprocal space.

At this point it is appropriate to mention two schools of thought regarding lattice sum methods which are closely related to the present method. One such school was originated by Ewald[16] and given recent extensive development by Nijboer and deWette in a series of papers, the principle one of which is footnoted.[17] In this school, the singularities are replaced by broadened functions with Gaussian forms thus introducing a convergence factor into the $A(\mathbf{h})$. The "tails" of these functions overlap the expansion point, and their effect must be compensated; the result is a "double series" method involving summations both in real space and reciprocal space. The procedure can be adjusted to make both sums converge with reasonable rapidity or to sacrifice rapidity of convergence in one sum in order to enhance this property in the other. The double series method can, in this way, be effectively transformed into a "single series" method with arbitrarily small residual error. In the second school, represented by Bertaut,[18] Jones and Templeton,[19] and Kanamori,[20] each singularity is replaced by a broadened function which vanishes identically outside a certain sphere concentric with the site of the singularity. By choosing the radius of this sphere correctly, the overlap effect can be eliminated entirely and a rigorous single series formulation obtained.

In the present method, there is no deliberate modification of the original physical model; the procedure for accelerating the convergence of (A6) is entirely mathematical in inspiration. Under this procedure, both sides of (A6) are rendered regular within an r_0 neighborhood of the origin by multiplying by r^{l+1}; then a repeated integration technique is invoked in order to improve the convergence. The result is a rigorous single series method with the following advantages: (1) only one transcendental function of h needs to be evaluated at

[16] P. P. Ewald, Ann. Physik **64**, 253 (1921).
[17] B. R. A. Nijboer and F. W. deWette, Physica **23**, 309 (1957).
[18] F. Bertaut, J. phys. radium **13**, 499 (1952).
[19] R. E. Jones and D. H. Templeton, J. Chem. Phys. **25**, 1062 (1956).
[20] J. Kanamori *et al.*, J. Phys. Soc. Japan **10**, 93 (1955).

each lattice point, and (2) this function becomes oscillatory at large real argument as well as small in magnitude thus minimizing the termination error. The function in question, $\Lambda_\nu(z)$, is discussed in detail below.

To continue with the derivation, let the terms in (A6) be rearranged, and let both sides be multiplied by the factor suggested above:

$$C_l^m r^{2l+1} = -B_l^m + (2\pi/3)\rho_0\delta_{0l} r^{l+3} + \xi_l^m \sum_{\mathbf{h}} \frac{A(\mathbf{h})}{(2\pi h)^2} r^{l+1} j_l(2\pi hr) P_l^{|m|}(\cos\theta_{\mathbf{h}}) \times \exp(-im\phi_{\mathbf{h}}). \quad \text{(A7)}$$

Here the compact notation ξ_l^m is defined by

$$\xi_l^m = 4\pi i^l (2l+1)(l-|m|)!/(l+|m|)!. \quad \text{(A8)}$$

The following indefinite integral follows from the properties of the spherical Bessel functions:

$$\int z^{l+1} j_l(z) z\,dz = z^{l+2} j_{l+1}(z) + \text{const.} \quad \text{(A9)}$$

Using (A9), and applying $\int_0^r \cdots r dr$ to both sides of (A7), one obtains

$$C_l^m \frac{r^{2l+3}}{2l+3} = -B_l^m \frac{r^2}{2} + \frac{2\pi}{3}\rho_0\delta_{0l}\frac{r^{l+5}}{l+5} + \xi_l^m \sum_{\mathbf{h}} \frac{A(\mathbf{h})}{(2\pi h)^3} r^{l+2} j_{l+1}(2\pi hr) \times P_l^{|m|}(\cos\theta_{\mathbf{h}}) \exp(-im\phi_{\mathbf{h}}). \quad \text{(A10)}$$

If this same operation is applied a total of n times,

$$C_l^m \frac{r^{2l+2n+1}}{(2l+3)(2l+5)\cdots(2l+2n+1)} = -B_l^m \frac{r^{2n}}{2\cdot 4\cdot 6\cdots 2n} + \frac{2\pi}{3}\rho_0\delta_{0l}\frac{r^{l+2n+3}}{(l+5)(l+7)\cdots(l+2n+3)} + \xi_l^m \sum_{\mathbf{h}} \frac{A(\mathbf{h})}{(2\pi h)^{2+n}} r^{l+1+n} j_{l+n}(2\pi hr) P_l^{|m|}(\cos\theta_{\mathbf{h}}) \times \exp(-im\phi_{\mathbf{h}}). \quad \text{(A11)}$$

The following notation,[21]

$$(a)_n = a(a+1)(a+2)\cdots(a+n-1) = \Gamma(a+n)/\Gamma(a), \quad \text{(A12)}$$

will be used and (A11) solved for C_l^m. Thus:

$$C_l^m = -B_l^m \frac{(l+\frac{3}{2})_n}{n!} r^{-(2l+1)} + \frac{2\pi}{3}\rho_0\delta_{0l}\frac{(l+\frac{3}{2})_n}{((l+5)/2)_n} r^{2-l} + 2^n (l+\tfrac{3}{2})_n \xi_l^m \sum_{\mathbf{h}} A(\mathbf{h}) \frac{(2\pi h)^{l-2} j_{l+n}(2\pi hr)}{(2\pi hr)^{l+n}} \times P_l^{|m|}(\cos\theta_{\mathbf{h}}) \exp(-im\phi_{\mathbf{h}}). \quad \text{(A13)}$$

[21] A. Erdelyi (Bateman Manuscript Project), *Higher Transcendental Functions* (McGraw-Hill Book Company, Inc., New York, 1953), Vol. I, p. 302.

The function $\Lambda_\nu(z)$ is defined[22] by

$$\Lambda_\nu(z) = 2^\nu \Gamma(1+\nu) J_\nu(z)/z^\nu. \quad \text{(A14)}$$

Therefore,

$$\frac{j_\nu(z)}{z^\nu} = \frac{\Gamma(\frac{1}{2})}{2^{\frac{1}{2}}} \frac{J_{\nu+\frac{1}{2}}(z)}{z^{\nu+\frac{1}{2}}} = \frac{\Gamma(\frac{1}{2})}{2^{\nu+1}} \frac{\Lambda_{\nu+\frac{1}{2}}(z)}{\Gamma(\nu+\frac{3}{2})}. \quad \text{(A15)}$$

The variable r may now be given a fixed value r_1 and the final expression for C_l^m becomes

$$C_l^m = -B_l^m \frac{(l+\frac{3}{2})_n}{n!} r_1^{-(2l+1)} + \frac{\pi\rho_0\delta_{0l} r_1^2}{\frac{3}{2}+n} + \frac{\xi_l^m}{2^l(\frac{3}{2})_l} \sum_{\mathbf{h}} A(\mathbf{h})(2\pi h)^{l-2} \Lambda_{n+l+\frac{1}{2}}(2\pi hr_1) \times P_l^{|m|}(\cos\theta_{\mathbf{h}}) \exp(-im\phi_{\mathbf{h}}). \quad \text{(A16)}$$

Although this formula appears complicated, it frequently becomes quite simple in specialized cases. Thus the first term on the right hand side vanishes, unless the singularity at the origin has a multipole component of the same species as that of the potential component being calculated and the second term vanishes for all cases in which the l value associated with this potential component is different from zero. Note that, in applying (A16), the analyst has two degrees of freedom of choice in that he can set r_1 equal to any value in the open continum $0 < r_1 < r_0$ and n equal to any integer in the range $0 \leqslant n < \infty$. Values of r_1 near to r_0 are advantageous since they result in fewer terms to be summed. To choose a value of n intelligently, one must take into account the properties of the functions $\Lambda_\nu(z)$ for real argument, and the over-all accuracy required in the calculation. For high orders, $\Lambda_\nu(x)$ is characterized by a bell-shaped central maximum, and oscillatory skirts. Quantitatively, as $x \to 0$,

$$\Lambda_\nu(x) \sim \exp[-x^2/4(\nu+1)], \quad \text{(A17)}$$

and as $x \to \infty$,

$$\Lambda_\nu(x) \sim \frac{2^{\nu+\frac{1}{2}}\Gamma(1+\nu)\cos[x-(\nu+\frac{1}{2})\pi/2]}{\Gamma(\frac{1}{2})x^{\nu+\frac{1}{2}}}. \quad \text{(A18)}$$

After x exceeds ν, the negative power of x in (A18) overcomes the large constant factors, and (A16) converges more or less quickly depending upon the value of ν. Briefly, a large value of ν postpones the onset of convergence but makes the convergence more rapid once it begins; it is recommended when high accuracy is desired. Tables of $\Lambda_\nu(x)$ for half-integer order are given in a reference already cited.[22] In addition, a ten

[22] A. N. Lowan *et al.*, *Tables of Spherical Bessel Functions* (Columbia University Press, New York, 1943), Vol. II, p. 213.

decimal table of $\Lambda_{45/2}(u^{\frac{1}{2}})$ has been constructed and is acknowledged in Sec. VII. The argument in this table, which is actually equal to $(2\pi hr_1)^2$, covers the range from 0.0 to 1600.0 in steps of 0.1. This form of argument has proved extremely useful, especially since the square of $(2\pi hr_1)$ is obtained more easily than the first power of this quantity. There is every reason to believe that the processes of function generation and lattice summation can be incorporated into the same automatic digital computer routine; such a step will be attempted as soon as it is justified by the volume of work. For a limited number of calculations, however, the use of the Λ table is recommended.

Returning to a consideration of the *nonuniform* background charge density ρ', one can say of the potential V' generated by ρ'

$$V'=\sum_{l=0}^{\infty}\sum_{m=-l}^{l}\sum_{k=0}^{\infty}C'_{lk}{}^{m}r^{l+2k}P_l^{|m|}(\cos\theta)e^{im\phi}. \quad \text{(A19)}$$

The reasons for the exact form of this expansion will become clear presently. Note that the terms with $k=0$ constitute the Laplacian portion of V', those with $k>0$, the non-Laplacian. Thus, of all the terms associated with a particular surface harmonic, that is, with an angular dependence indicated by a particular set of numbers l and m, the Laplacian term is the most important in a neighborhood of the origin.

By repeating the technique employed earlier, it is easy to show that

$$\sum_{k=0}^{\infty}C'_{lk}{}^{m}r^{l+2k}=\xi_l{}^{m}\sum_{\mathbf{h}}\frac{A'(\mathbf{h})}{(2\pi h)^2}j_l(2\pi hr)\times P_l^{|m|}(\cos\theta_{\mathbf{h}})\exp(-im\phi_{\mathbf{h}}). \quad \text{(A20)}$$

The power series development for the spherical Bessel function is as follows:

$$\begin{aligned}j_l(z)&=\left(\frac{\pi}{2z}\right)^{\frac{1}{2}}\left(\frac{z}{2}\right)^{l+\frac{1}{2}}\sum_{k=0}^{\infty}\frac{(-1)^k(z/2)^{2k}}{\Gamma(k+1)\Gamma(k+1+l+\frac{1}{2})};\\&=\sum_{k=0}^{\infty}\frac{(-1)^k\Gamma(\frac{3}{2})}{2^{l+2k}\Gamma(k+l+\frac{3}{2})k!}z^{l+2k};\\&=\sum_{k=0}^{\infty}\frac{(-1)^k}{2^{l+2k}(\frac{3}{2})_{l+k}k!}z^{l+2k}. \quad \text{(A21)}\end{aligned}$$

By equating like powers of r in (A20), one finds that

$$C'_{lk}{}^{m}=\frac{\xi_l{}^{m}(-1)^k}{2^{l+2k}(\frac{3}{2})_l k!}\sum_{\mathbf{h}}A'(\mathbf{h})(2\pi h)^{l-2+2k}\times P_l^{|m|}(\cos\theta_{\mathbf{h}})\exp(-im\phi_{\mathbf{h}}). \quad \text{(A22)}$$

The procedure for finding the potentials V and V' generated by the given charge distributions ρ and ρ' has now been fully developed. It may be helpful, therefore, to consider the total potential or sum of V and V' as partitioned into the self-potential V_S of the singularity at the origin and the potential V_0 at the site of the origin due to all other charge. Thus:

$$V_T=V+V'=V_S+V_0. \quad \text{(A23)}$$

Evidently, V_T is simply the sum of (A3) and (A19), and V_0 is this same sum with the $B_l{}^m$ terms deleted. Thus, in surface harmonic expansion, one has

$$V_0=\sum_{l=0}^{\infty}\sum_{m=-l}^{l}\left[-\frac{2\pi}{3}\rho_0\delta_{0l}r^2+C_l{}^{m}r^l+\sum_{k=0}^{\infty}C'_{lk}{}^{m}r^{l+2k}\right]\times P_l^{|m|}(\cos\theta)e^{im\phi}. \quad \text{(A24)}$$

This is the potential with which the singularity at the origin can interact energetically, and, in most cases, the interactions with the non-Laplacian terms can be neglected in favor of the interactions with the Laplacian terms. Practically, this means that usually only the $C_l{}^m$ and the $C'_{l0}{}^m$ coefficients will ever have to be calculated.